HHS Public Access

Author manuscript

Opt Lett. Author manuscript; available in PMC 2024 June 18.

Published in final edited form as:

Opt Lett. 2023 April 15; 48(8): 1994–1997. doi:10.1364/OL.480896.

High-speed measurement of retinal arterial blood flow in the living human eye with adaptive optics ophthalmoscopy

Ruixue Liu[1], **Xiaolin Wang**[1], **Sujin Hoshi**[1,2,3], **Yuhua Zhang**[1,2,*]

[1]Doheny Eye Institute, 150 N Orange Grove Blvd, Pasadena, CA 91103

[2]Department of Ophthalmology, University of California - Los Angeles, 100 Stein Plaza Driveway, Los Angeles, CA 90024

[3]Department of Ophthalmology, University of Tsukuba, Ibaraki, Japan

Abstract

We present a technique to measure the rapid blood velocity in large retinal vessels with high spatiotemporal resolution. Red blood cell motion traces in the vessels were non-invasively imaged using an adaptive optics near-confocal scanning ophthalmoscope at a frame rate of 200 fps. We developed software to measure blood velocity automatically. We demonstrated the ability to measure the spatiotemporal profiles of the pulsatile blood flow with a maximum velocity of 95~156 mm/s, in retinal arterioles with a diameter > 100 μm. High-speed and high-resolution imaging increased the dynamic range, enhanced sensitivity, and improved the accuracy for studying retinal hemodynamics.

The human retinal vascular network consists of blood vessels with lumen diameters ranging from ~180 μm to 4 μm transporting blood flow with speer5d varying from ~ 200 mm/s to 0.1 mm/s, facilitating the essential metabolic activities of the inner retina [1]. An accurate assessment of retinal hemodynamics is necessary to understand normal physiologic processes and pathologic conditions in the retina and facilitate novel treatments for retinal diseases [2]. Various techniques have been developed to measure retinal blood flow and velocity in blood vessels of different lumen diameters [2]. Laser Doppler flowmetry (LDF) [3], laser speckle flowgraphy (LSF) [4], and Doppler optical coherence tomography (DOCT) [5] can measure blood velocity in vessels with a lumen diameter > 30 μm. Time-domain color DOCT ascertained the velocity profile of the blood flow across the lumen with micrometer-scale resolution in the imaging light direction [6]. Fourier-domain DOCT rendered continuous temporal variation of the blood velocity with improved imaging speed [7]. Adaptive optics (AO) ophthalmoscopy enabled diffraction-limited imaging allowing for in vivo precise measurement of the blood velocity in small vessels down to the finest capillaries in the human retina with a high spatial and temporal resolution, and characterized leukocyte, erythrocyte aggregates, and erythrocyte velocity and pulsatility [8–15].

*Corresponding author: yzhang@doheny.org.

Disclosures. The authors declare no conflicts of interest.

While in vivo measurement of the blood flow in the smallest to largest retinal vessels has become possible in animal eyes [16–18], precise measurement of the rapid temporal and spatial variation of the blood flow in large retinal arterioles, which can be > 100 mm/s during the systolic phase [2], remains challenging. Ultrahigh-speed swept source OCT with a scan rate of 400 kHz and sophisticated phase unwrapping has been demonstrated with the potential to measure blood velocity up to 100 mm/s [19, 20]. AO scanning laser ophthalmoscopy (AOSLO), by stopping its slow scanner across a selected vessel during the frame scanning, can generate the spatiotemporal (ST) motion traces of red blood cells, thereby allowing for direct measurement of the blood velocity across the lumen [14, 15]. However, the maximum measurable blood velocity was limited by the frame rate [15]. In this study, we present a method using an adaptive optics near-confocal scanning ophthalmoscope (AONCO) to measure the temporal and spatial profiles of the blood flow in the primary retinal arterioles with a lumen diameter > 100 μm near the optic nerve head (ONH).

We have reported the AONCO previously [13, 21]. It operates with a line scan near confocal imaging mechanism that employs a near infrared (NIR) low coherence superluminescent diode (λ = 795 nm) as the imaging light source and uses a high-speed line camera to acquire the retinal image through an anamorphic imaging mechanism. The line camera acts as a confocal gate rejecting out-of-focus scattering light. The AONCO acquires images in the living human retina over a field of view of 1.2° × 1.2° at a frame rate of 200 fps. In this study, we programmed the scanner to stop at the selected vessels in the frame, as reported by Zhong et al. [14, 15], allowing for 102.40 kHz repeated acquisition of the intersectional area. The partial image acquired during this scanner stationary period rendered the motion traces of the red blood cells. Then, the scanner returned to the frame top after a pause (< 2.5 ms) and started scanning for the next frame.

As illustrated in Fig. 1(a) & (b), the ST trace angle θ provides a measurement of the horizontal velocity V_x of a red blood cell,

$$V_x = nl_p/(mt_p) = l_p/t_p \cot\theta = l_p l_r \cot\theta \quad (1)$$

where n and m are pixel numbers in the spatial and temporal directions of the partial image, respectively. l_p is the pixel spatial size (0.7μm/pixel), t_p is the line period, and l_r is the line rate. For a ST trace image consists of 512 lines with ~360 μm field of view, the measurement range is 0.14 mm/s (n=1, m=512) to 36,864 mm/s (n=512, m=1) with a frame rate of 200 fps. The maximum speed can only be measured in a vessel parallel to the scanning line, whereas the minimum velocity is limited by the noise. Assuming the angle between the vessel and the scanning line is α, the velocity in the blood vessel is $V = V_x/\cos\alpha$. Assuming the scanning light line width is D_s, which equals the Airy disk diameter of the imaging light focusing on the retina (4.8 μm in this study), when a red blood cell moves across the scan line, the velocity in the vertical direction is,

$$V_y = D_s/(mt_p)$$

(2)

With Eq. (1) and Eq. (2), we obtain a new equation describing the relationships between the velocity, the scanning line rate f_l, and the trace characteristics.

$$V = D_s f_l / (m \sin \alpha)$$

(3)

Apparently, a higher line rate allows us to measure a faster flow, i.e., increases the measurement range. For a segment of a ST trace whose angle can be measured, the trace should be at least across two scanning lines. In fact, the ST trace must be across multiple scanning lines to ensure a reliable measurement. For a vessel with $\alpha = 60°$, if $m = 4$, the maximum measurable velocities at 30, 60, 100, and 200 fps are 21.3, 42.8, 70.9, and 141.5 mm/s, respectively (Fig. 1(c)). Fig. 2 illustrates ST traces gained increased slope, i.e., improved measurement sensitivity, with faster frame rates.

During the image acquisition, the imaging and wavefront sensing light power were 0.5 mW and 25 μW, respectively, corresponding to a composite of 0.34 times the ANSI maximum permissible exposures (MPE) under the condition of 1 hour of continuous exposure [21]. The pupil of the participant was dilated with 1.0% tropicamide and 2.5% phenylephrine hydrochloride. The participant's head was aligned and stabilized using a head-mount. A fixation target directed the participant's view angle.

We developed an algorithm to measure the average angle of the FFT of the ST traces using the second-order moments, in the following steps. First, we registered consecutive frames based on the upper partial images. Next, we enhance the contrast of the ST traces by removing the uneven background in individual frame using the method reported by Duncan et al. [22]. Then, we divided the vessel cross-section into multiple segments (Fig 3(a)–(b)) and performed the FFT for every segment. The FFT of the ST traces typically had an oval shape (Fig 3(c)). The orientation angle represents an average slope of multiple traces. To extract the spectral component of the ST traces, we removed the high-frequency components with spectral intensity < mean + 2 × standard deviation (Fig 3(d)). Finally, we measured the orientation angle of the retained FFT image using second-order moments [23] (Fig 3(e)) and calculate the velocity by Eq. (1).

To evaluate the accuracy, we compared the ST trace angles obtained using the software and by manual measurement in 30 image segments. The two methods highly agree with each other (Fig (4)). Fig. 5 demonstrates the blood velocity measured in an arteriole with a lumen diameter of 110 μm near the ONH. Over time, the velocity manifested a clear cardiac-dependent pulsation. Across the lumen, the blood flew with a quasi-parabolic velocity profile [24]. The centerline velocity varied from 95 to 156 mm/s in multiple cardiac cycles, whereas the lowest velocity at the end of the diastole phase ranged from 10~20 mm/s (Fig. 6 (a)). High-speed imaging enabled the velocity waveform to be measured continuously with a high temporal resolution, thereby allowing for calculating the flow acceleration within the

cardiac cycles. Fig. 6 shows the blood velocity and acceleration along the center line and near the vessel wall over time.

In a pioneering work, Zhong et al. measured blood velocity up to 70 mm/s in retinal arterioles using an AOSLO [25]. The maximum measurable blood velocity was limited by the AOSLO's frame rate (30 – 56 fps), essentially, the line scan speed (16 – 20 KHz) [14, 25]. In this study, AONCO imaged red blood cell motion traces at 200 fps (the line rate was 102.4 KHz) with a line scan mechanism that does not cause sinusoidal distortion, thereby generating the retinal structure and motion traces with high fidelity. High-speed and high-resolution imaging enhanced the ability to render the motion traces of the fast flowing red blood cells (Fig. 2), improving the accuracy for measuring the spatiotemporal profiles of the rapid blood flow (Figs. 4 & 5). Particularly, high-speed imaging can measure fast blood flow in vessels with large angles to the scanning line. Although the angle between the vessel and the scanning line may be reduced by rotating the optical system, it adds system complexity. Moreover, AONCO acquires an image within 5 ms, reducing eye movement caused distortion [26] and improving the measurement accuracy.

Our results are comparable with the published data. (Table 1). Since previous studies could only report spatially (across the lumen) or temporally (over the cardiac cycle) averaged velocity owing to limited spatial or temporal resolution, we converted our data to mean velocities over a cardiac cycle $<V_t>$, and over both the cardiac cycle and lumen cross-section $<V_{ts}>$. Our study's peak systolic velocity V_{max}, the temporal average $<V_t>$, and the spatiotemporal average $<V_{ts}>$ agreed with previous publications. However, our study's average systolic velocity averaged over the lumen cross-section $<V_s>$ was higher. This difference may be due to the different temporal imaging resolutions. Prolonged spatiotemporal integration can suppress the high-amplitude data.

High spatiotemporal resolution measurement of the blood velocity allows for a fine characterization of the hemodynamics within a cardiac cycle thereby revealing the mechanics driving the fluid, the arterial compliance, and the flow resistance [31]. The wall shear stress (WSS) is crucial in regulating endothelial function [2, 32]. Current estimates of the WSS have relied mainly on the time-averaged velocity [33]. In vitro studies have found that the accelerating and steady blood flow regulates short- and long-term endothelial function via independent biomechanical pathways [34]. Clinical trials of flow-mediated dilation of the brachial artery indicated that the time-averaged velocity could not fully characterize the shear stimulus, and the transient acceleration was an independent variable governing the shear stimulus [31, 35]. Our method can precisely measure the waveform of blood velocity within a cardiac cycle, thereby potentially estimating the shear stress exerted on the vessel wall by accurately characterizing the acceleration near the endothelial surface (Fig. 6). Thus, our future work will characterize the higher-order dynamic properties of the pulsatile flow in retinal arterioles across different regions thereby obtaining critical hemodynamic parameters for assessing the flow viscosity and vessel wall shear stress. Further, we will investigate alterations of the higher-order hemodynamic properties in different physiological processes, e.g., visual stimulation or gas breathing perturbations, and in systemic conditions such as hypertension and diabetes. Alterations in microcirculation, as may occur in diabetic retinopathy, glaucoma, age-related macular

degeneration, hypertension, stroke, and Alzheimer's disease, can result in a malfunction of the retinal vascular network and lead to retinal tissue damage and functional impairment [2]. Our method enhances the ability to detect flow alterations, which could signify a malfunction of the retinal microcirculation at an early stage.

We have identified limitations that can be addressed in future development. For example, the overlapping spatiotemporal traces of a large number of red blood cells in the depth of field of the AONCO can cause measurement errors. This drawback can be mitigated by novel strategy that improves the axial resolution, which is being developed in the lab. Meanwhile, although high-speed imaging extended the dynamic range for measuring the blood flow, the measurement is still restricted for the inferior and superior quadrants where blood vessels may be perpendicular to the fast scan line. Thus, a mechanism that can adjust the angle between the fast scan and the vessel is highly desirable. Further, a retinal tracker can be crucial for imaging patients with degraded fixation stability thus it should be implemented in the system.

In conclusion, high-speed and high-resolution imaging increased the dynamic range, enhanced the sensitivity, and improved the accuracy for measuring the spatiotemporal profiles of the rapid blood flow in large retinal arterioles, demonstrating the ability to study the fluid dynamics precisely within the cardiac cycle and potentially assessing retinal vascular health.

Funding.

National Institutes of Health (R01EY024378, R01EY034218), W. F. Keck Foundation, Carl Marshall Reeves & Mildred Almen Reeves Foundation, and Research to Prevent Blindness/Dr. H. James and Carole Free Catalyst Award for Innovative Research Approaches for AMD.

Data availability.

Data underlying the results presented in this paper are not publicly available at this time but may be obtained from the authors upon reasonable request.

References

1. Pournaras CJ, and Riva CE, Ophthalmologica 229, 61–74 (2013). [PubMed: 23257770]
2. Burns SA, Elsner AE, and Gast TJ, Annu Rev Vis Sci 7, 129–153 (2021). [PubMed: 34171198]
3. Riva CE, Grunwald JE, Sinclair SH, and Petrig B, Invest Ophthalmol Vis Sci 26, 1124–1132 (1985). [PubMed: 4019103]
4. Nagahara M, Tamaki Y, Tomidokoro A, and Araie M, Invest Ophthalmol Vis Sci 52, 87–92 (2011). [PubMed: 20702824]
5. Leitgeb RA, Werkmeister RM, Blatter C, and Schmetterer L, Prog Retin Eye Res 41, 26–43 (2014). [PubMed: 24704352]
6. Yazdanfar S, Rollins AM, and Izatt JA, Arch Ophthalmol 121, 235–239 (2003). [PubMed: 12583790]
7. White B, Pierce M, Nassif N, Cense B, Park B, Tearney G, Bouma B, Chen T, and de Boer J, Opt Express 11, 3490–3497 (2003). [PubMed: 19471483]
8. Martin JA, and Roorda A, Ophthalmology 112, 2219–2224 (2005). [PubMed: 16257054]
9. Tam J, Tiruveedhula P, and Roorda A, Biomed Opt Express 2, 781–793 (2011). [PubMed: 21483603]

10. Bedggood P, and Metha A, Biomed Opt Express 3, 3264–3277 (2012). [PubMed: 23243576]
11. Arichika S, Uji A, Hangai M, Ooto S, and Yoshimura N, Invest Ophthalmol Vis Sci 54, 4394–4402 (2013). [PubMed: 23716632]
12. de Castro A, Huang G, Sawides L, Luo T, and Burns SA, Opt Lett 41, 1881–1884 (2016). [PubMed: 27082369]
13. Gu B, Wang X, Twa MD, Tam J, Girkin CA, and Zhang Y, Biomed Opt Express 9, 3653–3677 (2018). [PubMed: 30338146]
14. Zhong Z, Petrig BL, Qi X, and Burns SA, Opt express 16, 12746–12756 (2008). [PubMed: 18711513]
15. Zhong Z, Song H, Chui TY, Petrig BL, and Burns SA, Invest Ophthalmol Vis Sci 52, 4151–4157 (2011). [PubMed: 21467177]
16. Guevara-Torres A, Joseph A, and Schallek JB, Biomed Opt Express 7, 4228–4249 (2016). [PubMed: 27867728]
17. Joseph A, Guevara-Torres A, and Schallek J, Elife **8** (2019).**8**
18. Dholakia KY, Guevara-Torres A, Feng G, Power D, and Schallek J, Invest Ophthalmol Vis Sci 63, 18 (2022).
19. Baumann B, Potsaid B, Kraus MF, Liu JJ, Huang D, Hornegger J, Cable AE, Duker JS, and Fujimoto JG, Biomed Opt Express 2, 1539–1552 (2011). [PubMed: 21698017]
20. Lee B, Novais EA, Waheed NK, Adhi M, Talisa E, Cole ED, Moult EM, Choi W, Lane M, and Baumal CR, JAMA ophthalmology 135, 244–251 (2017). [PubMed: 28196198]
21. Lu J, Gu B, Wang X, and Zhang Y, Opt Lett 41, 3852–3855 (2016). [PubMed: 27519106]
22. Duncan DD, Lemaillet P, Ibrahim M, Nguyen QD, Hiller M, and Ramella-Roman J, J Biomed Opt 15, 056014 (2010). [PubMed: 21054108]
23. Hu M-K, IRE transactions on information theory 8, 179–187 (1962).
24. Bishop JJ, Nance PR, Popel AS, Intaglietta M, and Johnson PC, Am J Physiol Heart Circ Physiol 280, H222–236 (2001). [PubMed: 11123237]
25. Zhong Z, Huang G, Chui TY, Petrig BL, and Burns SA, J Vis 12, 3 (2012).
26. Lu J, Gu B, Wang X, and Zhang Y, Opt Express 26, 14356–14374 (2018). [PubMed: 29877476]
27. Feke GT, Tagawa H, Deupree DM, Goger DG, Sebag J, and Weiter JJ, Invest Ophthalmol Vis Sci 30, 58–65 (1989). [PubMed: 2643588]
28. Wang Y, Fawzi AA, Varma R, Sadun AA, Zhang X, Tan O, Izatt JA, and Huang D, Invest Ophthalmol Vis Sci 52, 840–845 (2011). [PubMed: 21051715]
29. Dai C, Liu X, Zhang HF, Puliafito CA, and Jiao S, Invest Ophthalmol Vis Sci 54, 7998–8003 (2013). [PubMed: 24222303]
30. Blatter C, Coquoz S, Grajciar B, Singh AS, Bonesi M, Werkmeister RM, Schmetterer L, and Leitgeb RA, Biomed Opt Express 4, 1188–1203 (2013). [PubMed: 23847742]
31. Stoner L, Young JM, Fryer S, and Sabatier MJ, Int J Vasc Med 2012, 589213 (2012). [PubMed: 22315688]
32. Davies PF, Nat Clin Pract Cardiovasc Med 6, 16–26 (2009). [PubMed: 19029993]
33. Samijo SK, Willigers JM, Brands PJ, Barkhuysen R, Reneman RS, Kitslaar PJ, and Hoeks AP, Ultrasound Med Biol 23, 583–590 (1997). [PubMed: 9232767]
34. Frangos JA, Huang TY, and Clark CB, Biochem Biophys Res Commun 224, 660–665 (1996). [PubMed: 8713104]
35. Stoner L, and McCully KK, Ultrasound Med Biol 38, 580–592 (2012). [PubMed: 22342687]

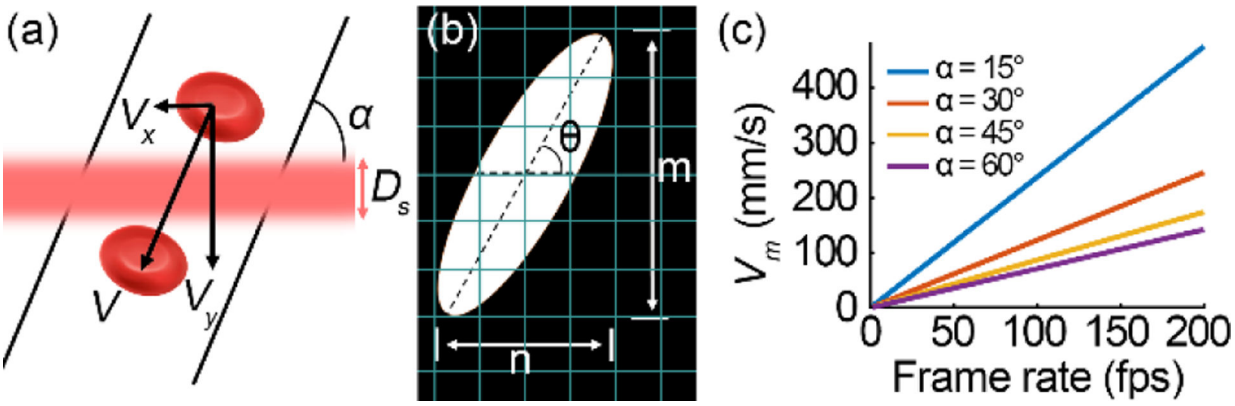

Fig. 1.

Estimating the maximum measurable blood velocity. (a) An illustration of a red blood cell in a vessel flowing across the scan line. (b) The motion trace of the red blood cell on the image. (c) The maximum measurable velocity (V_m) under different frame rates and various vessel orientation angles (α).

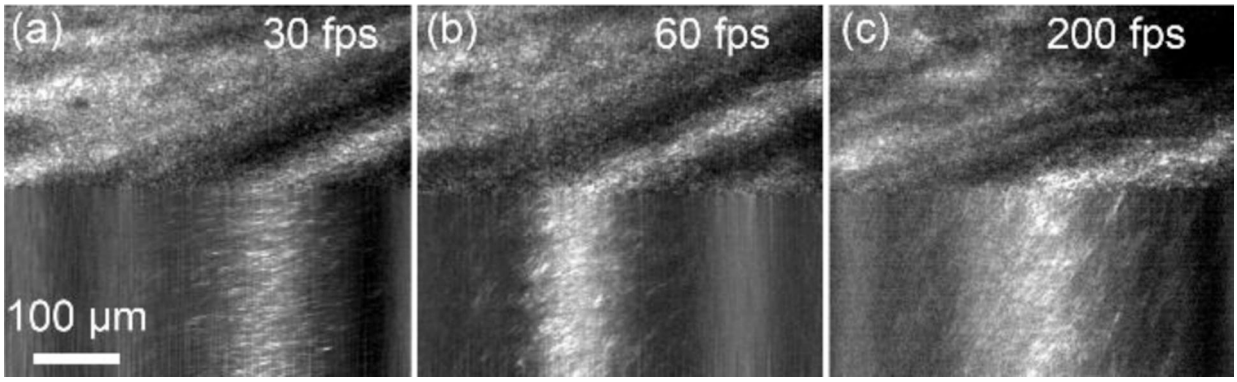

Fig. 2.

The red blood cell motion traces in a retinal arteriole imaged by the AONCO with different frame rates at the peak speed of the systolic phase. (a) 30 fps, (b) 60 fps, and (c) 200 fps.

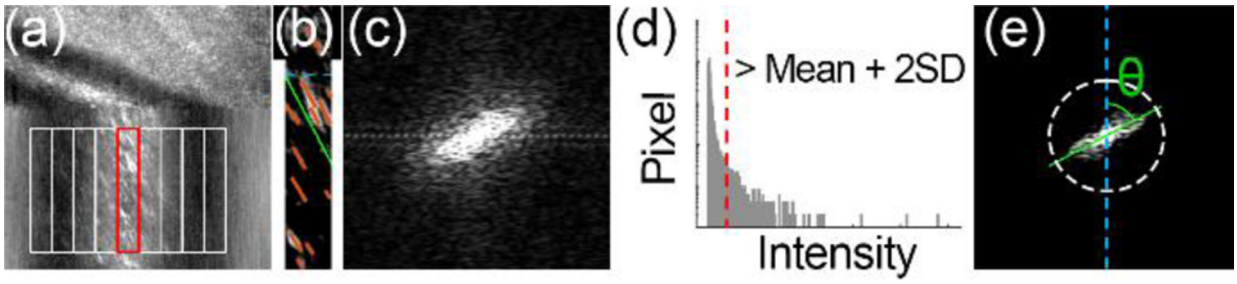

Fig. 3.

Automatic motion traces angle measurement. (a) The cross-section of the vessel is divided into a series of segments to calculate the velocity across the lumen. (b) Red blood cell motion traces in a single segment. (c) Fast Fourier Transform (FFT) of panel (b). (d) The spectral intensity of panel (c). The dashed red line indicates low-intensity noise to be removed. (e) The FFT image after noise reduction. The angle indicated by the green line represents the mean velocity of red blood cells in this segment. White ring delimits the reserved spectral components after removing the low-intensity noise, indicating the minimum resolvable spatial grating spacing is ~2.8 μm.

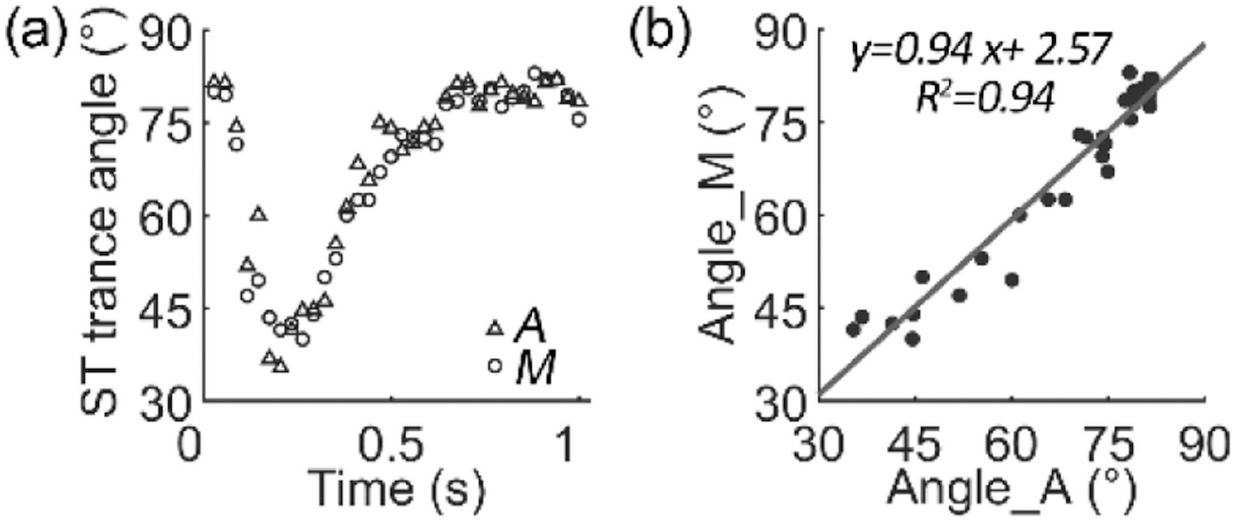

Fig. 4.

(a) Comparison of the orientation angles measured manually (M) and automatically (A). (b) The regression between angles measured automatically and manually. The 95% confidence interval of the slope is 0.86 to 1.03 and the intercept is −3.43 to 8.56.

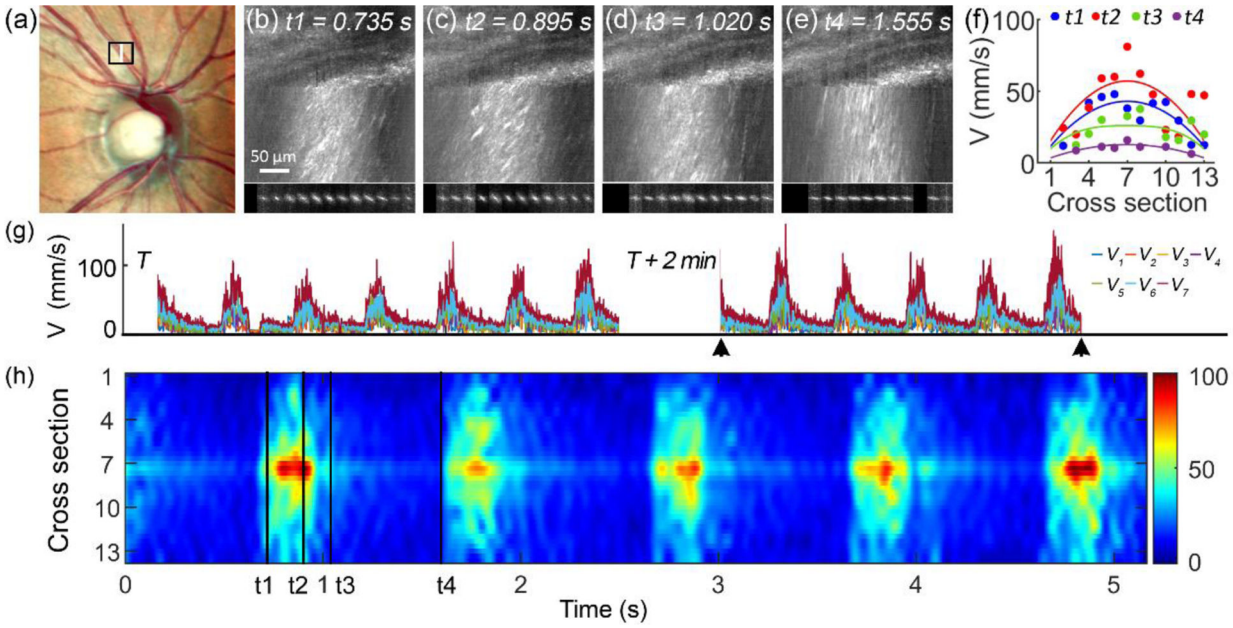

Fig. 5.

Blood velocity measured in a retinal arteriole with a lumen diameter of 110 μm. (a) Black box in the fundus photo delimits the AONCO imaging area. White line indicates the position where the scanner stopped. (b) – (e) Retinal images acquired at different phases within a cardiac cycle. Blood velocity was measured in 13 segments across the lumen. Underneath penls show the Fast Fourier transform of the blood flow in the 13 segments. (f) The velocity profiles measured at the 4 time points (shown in panels (b) - (e)) were fitted with the formula reported by Bishop et al. [24]. (g) Blood velocity measured in 2 imaging sessions with a time interval of 2 minutes. Color lines represent blood velocity measured at different lumen locations, from near the vessel wall (V_1) to the center line (V_7). (h) The spatial-temporal fluctuation of the blood flow in 5 cardiac cycles shown in panel (g) marked by black arrowheads. Color bar dimension is mm/s. t1, t2, t3, and t4 indicate the time points shown in panels (b) to (e). The data were acquired in an eye of a 57 years old female participant with normal chorioretinal health.

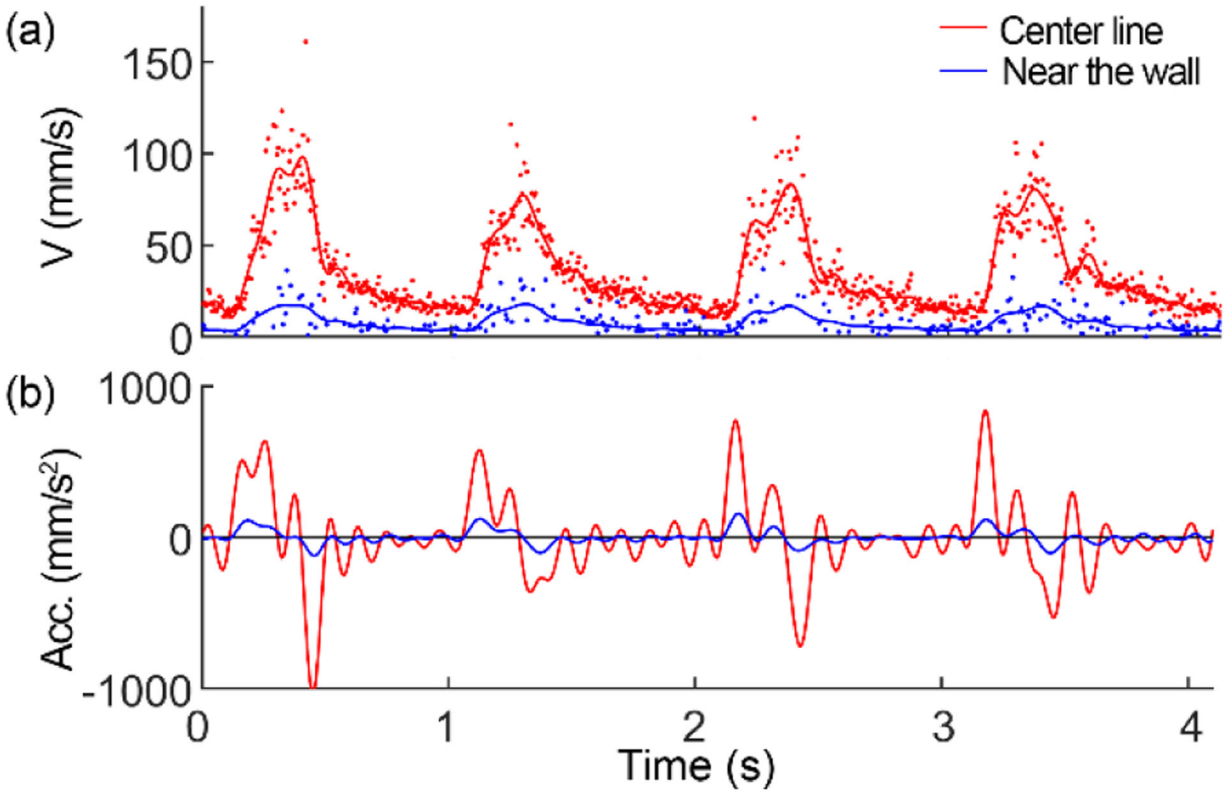

Fig. 6.
Blood velocity (a) and acceleration (b) at the center line and near the blood vessel wall.

Table 1

Blood velocities in retinal arterioles by methods

Method	Lumen (μm)	V_{max} (mm/s)	$\langle V_t \rangle$ (mm/s)	$\langle V_s \rangle$ (mm/s)	$\langle V_{ts} \rangle$ (mm/s)
AONCO	110	95.0 – 156.0	33.1 – 39.8	48.2 – 59.2	18.9 – 24.3
LDF [27]	123	109.0 ± 20.0			
LDF [3]	39 – 134		7.0 – 36.0		
LSF [4]	120 ± 16		41.7 ± 4.2		
DOCT [19]	NOD[a]			25.8 – 35.6	
DOCT [28]	NOD				24.6 ± 4.0
DOCT [29]	65 – 102				15.8 – 26.4
DOCT [30]	NOD			30.0 – 45.0	

[a]NOD: location near the optic disk.